SIMULATOR EXPERIMENTS FOR AEROELASTIC ROTORCRAFT-PILOT COUPLINGS

Andrea Zanoni
Department of Aerospace Science and Technology, Politecnico di Milano
Milano, Italy

Marek S. Lukasiewicz
Department of Aerospace Science and Technology, Politecnico di Milano
Milano, Italy

Pierangelo Masarati
Department of Aerospace Science and Technology, Politecnico di Milano
Milano, Italy

Michele Zilletti
Leonardo Helicopters Division
Samarate (VA), Italy

ABSTRACT

Rotorcraft pilot couplings, particularly pilot-assisted oscillations, result from interactions between pilot biomechanics and vehicle dynamics, potentially causing instabilities. Traditional stability analysis uses simplified biodynamic feedthrough models, focusing on inter-pilot variability under standard conditions. However, biodynamic feedthrough varies with muscle activation, which changes based on task demands. This study employs a purposely-developed testbed to evaluate the biodynamic feedthrough in pilot-in-the-loop tests. Two scenarios were tested: maintaining leveled flight amid turbulence in degraded visual conditions and an ADS-33 vertical repositioning maneuver. Preliminary results indicate significant differences between closed-loop flight behavior and open-loop biodynamic feedthrough estimates, confirming task-dependent changes in pilot impedance. This work advances rotorcraft-pilot coupling risk assessment by capturing real-world pilot-vehicle coupling, moving beyond static biomechanical models.

Keywords: Rotorcraft Pilot Couplings, BioDynamic FeedThrough, Pilot-Assisted Oscillations, Flight Simulation.

INTRODUCTION

The study of Rotorcraft Pilot Couplings (RPC) involves understanding the complex interactions between pilots and their aircraft, particularly in adverse conditions that, if not properly accounted for, can lead to instabilities. Relatively high-frequency couplings, typically referred to as Pilot-Assisted Oscillations (PAO), involve the interplay between aeroelastic behavior of the vehicle and the pilot's body biomechanical response (Ref. 1). Predicting whether and how a rotorcraft design is prone to developing PAO phenomena is crucial to take action as early as possible, when the cost of interventions on the design is still manageable (Ref. 2).

A typical approach to this problem is to evaluate the stability of a feedback system constituted by a model of the relevant vehicle dynamics — generally including the rigid body motion and some low-frequency aeroelastic modes in the frequency range of typical biomechanical modes — with a simplified representation of the participating biomechanics of the pilot's body. The latter is typically represented by the input-output relationship between the vehicle accelerations and the control inceptors' motion they induce, i.e., the BioDynamic FeedThrough (BDFT). The method, while of undeniable value, can be considered skewed toward the verification of the design concerning the inter-subject variability of the BDFT, i.e., focused on ensuring adequate stability for different pilots placed in the *same* psycho-physical state, which is typically representative of standard operations by well-trained pilots.

However, the BDFT depends on the pilot's body biomechanical impedance in relation to control inceptors' motion, which in turn depends on the muscle activation levels, especially in the limbs. The muscle activation levels are modified by the pilot, sometimes consciously but most of the time in an unconscious manner, in response to different stimuli during the execution of a flight task. As a reference example, one can consider the case of routine operations performed in clear Visual Meteorological Conditions (VMC), as opposed to the case of an emergency operation conducted in the Degraded Visual Environment (DVE). The impedance of the pilot's body in the second case will likely be significantly higher than in the first one (Refs. 3–5).

An experimental setup has been developed to enable such evaluation of BDFT variability and its effects on the stability of the Pilot-Vehicle System (PVS) in pilot-in-the-loop tests. Unlike previous attempts (Ref. 6), the implementation of the flight mission scenarios was not performed on a conventional flight simulator, but rather on a dedicated experimental hardware, the RPC testbed (Ref. 7). This choice made it possible to focus more easily on the scenarios developed for RPC evaluation and to eventually perform *online* identification of the BDFT during the tests, as the RPC testbed motion platform can introduce the high-frequency excitations required as external disturbances.

PRELIMINARY INVESTIGATION

The pilot-inceptor system dynamics were identified ahead of the closed-loop tests with *open-loop* BioDynamic Feedthrough (BDFT) (Refs. 7, 8) identification tests. The identified transfer functions were put in a feedback loop with the Flight Dynamics Models (FDM)s to assess the stability of the PVS in reference conditions.

Experimental Setup

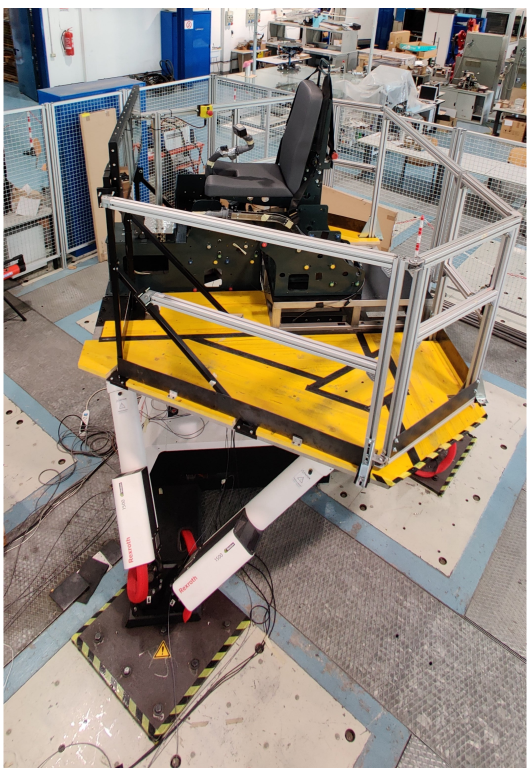

Figure 1. The RPC testbed.

The RPC testbed is an experimental facility that holds some similarities with a training flight simulator: it is composed of a 6 degrees of freedom motion platform and a simplified rotorcraft cockpit mockup. Conventional helicopter flight controls are employed, together with a glass cockpit setup. However, the pivot points of the control levers are easily reconfigurable and can be adapted to different flight control layouts. The motion base is capable of producing motion cueing feedback and higher-frequency signals.

Table 1. Geometric and inertial properties of the collective inceptor used for the BDFT identification tests.

Parameter	Symbol	Value	Units
Length	ℓ	350	mm
Mass	m_ℓ	2.2	kg
CG position	x_{CG}	330	mm
Moment of inertia	J_{CG}	0.3	$\mathrm{kg\,m^2}$

Table 2. Characteristics of the pilots participating in the tests. Only rotary-wing aircraft flight hours are indicated.

Parameter	NP-01	PP-02	Units
Sex	M	M	-
Age	25	59	y
Height	194	180	cm
Weight	89	69	kg
Flight experience	60	600	h

The test setup is completed by rotary Hall effect sensors (Active Sensors mod. MHR5542 CV-60) mounted on the collective and cyclic assemblies, a linear potentiometer measuring the travel of the left pedal (GEFRAN mod. PZ34-FF004391), and three MEMS accelerometers (Kistler mod. 8316A010A0AC03) located underneath the seat on its structure. Sensor signals are routed to a Siemens SCADAS acquisition system, which samples them at 1024 Hz.

The main properties of the collective inceptor installed during the identification tests are collected in Table 1.

Provisions have been taken to reduce as much as possible the friction acting on the collective control rotation. This choice allows nonlinearities in the pilot-control inceptor dynamics to be reduced, simplifying the BDFT identification.

The tests were conducted with two pilots: the first one, indicated as NP-01, is a non-professional pilot type-rated for the Robinson R44, with approximately 60 h of flight experience. The second one, indicated as PP-02, is a professional fixed-wing pilot, with approximately 18 000 h of flight experience on short, medium, and long-range airliners, and 600 h on rotary-wing aircraft. Their physical properties and flight experience are summarized in Table 2.

In this context, we will refer to *closed-loop* testing when the pilot is actively controlling the Flight Dynamics Model (FDM), and in turn receiving feedback signals, with visual and motion cueing. In contrast, *open-loop* testing will refer to cases in which the pilot is only subjected to a predefined motion excitation not modified in real-time by the vehicle dynamics.

BioDynamic FeedThrough Identification

Open-loop tests were conducted following established experimental procedures outlined in detail in previous publications (Ref. 7). The pilot is required to maintain a desired target collective input, within a tolerance of ±3 %, while subjected to a white noise vertical (Z-axis direction) acceleration input. The frequency range of the input is 0.5 Hz–7.5 Hz. The duration of each test run is 60 s and each testing point is repeated 3 times.

The target Frequency Response Function (FRF) to estimate the BDFT is the one relating the collective rotation $\delta_0(j\omega)$ (output) with the vertical acceleration $\ddot{Z}(j\omega)$ (input).

The acquired time series are split in 10 s records, with 50 % overlapping. On each record, the auto-spectrum $S_{\delta_0,\delta_0}(j\omega)$ of the output signal and the cross-spectrum between the output and the input signal $S_{\delta_0,\ddot{Z}}(j\omega)$ are computed, using the Welch method (Ref. 9). The Frequency Response Function estimate is then obtained via the H_1 estimator:

$$H_{\delta 0,\ddot{Z}}(j\omega) = \frac{S_{\delta_0,\delta_0}(j\omega)}{S_{\delta_0,\ddot{Z}}(j\omega)} \tag{1}$$

The experimental FRFs were then fitted to a simple model of the BDFT:

$$H_{\delta 0,\ddot{Z}}(j\omega) = \frac{\mu}{\omega_0^2}\frac{1+T_z s}{s(s^2+2\xi\omega_0 s+\omega_0^2)} \tag{2}$$

The two complex-conjugated poles $s_{1,2} = -\xi\omega_0 \pm j\sqrt{1-\xi^2}\omega_0$ represent the dominant dynamics of the left arm and the collective lever for the rotation of the collective lever. The pole in $s=0$ and the zero in $s=-1/T_z$ are tuned to enhance the asymptotic behavior of the transfer function at frequencies lower and higher than ω_0, and the gain μ/ω_0^2 sets its overall magnitude. This model has been presented in previous publications (Refs. 10, 11), in some cases with an added pure time delay term, enhancing the fitting of the phase. However, in this work, the pure delay term was discarded, since the phase fit was already satisfactory. Moreover, a pure delay term in a purely rational polynomial transfer function would require special treatment, e.g., via Padé approximations.

Two example results of the identified BDFTs for the pilots involved in the closed-loop tests are reported in Figures 2 and 3. It can be noted that overall, the fitting is satisfactory, as the global behavior due to the main pole associated with pilot biomechanics and inceptor dynamics is well-captured. However, especially with pilot NP-01, it can also be noted how some information is lost at higher frequencies, with the relative amplification peaking at about 6 Hz completely missed by the simplified model of Eq. (2). This is a known problem that is currently under investigation (Refs. 12, 13), and a revision of the modelization of the pilot biomechanics is probably necessary, since the behavior of the BDFT in the frequency range 5–7 Hz is likely to be significantly influenced by the first axial vibration mode of the pilot's spine (Ref. 14).

Table 3 shows the values of the BDFT model parameters resulting from the identification in every run that was performed with 80 % collective, the target position.

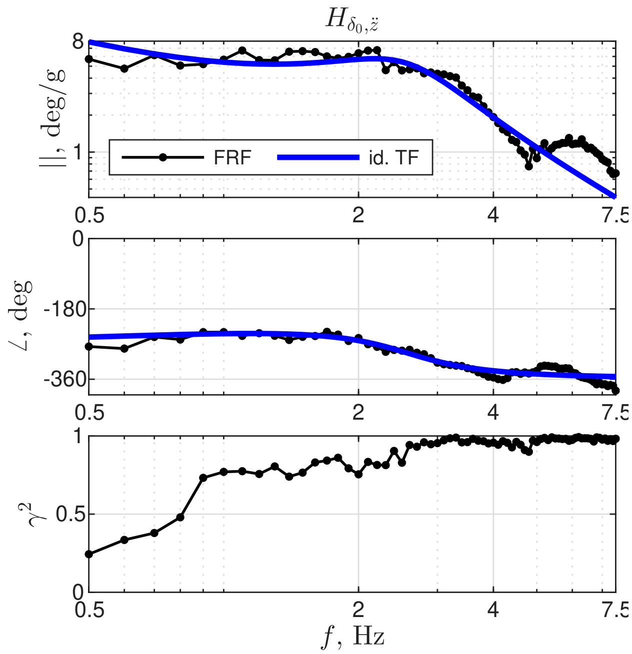

Figure 2. Experimental and identified BDFT transfer function for pilot NP-01. Experimental FRF: black line; identified BDFT transfer function: blue line.

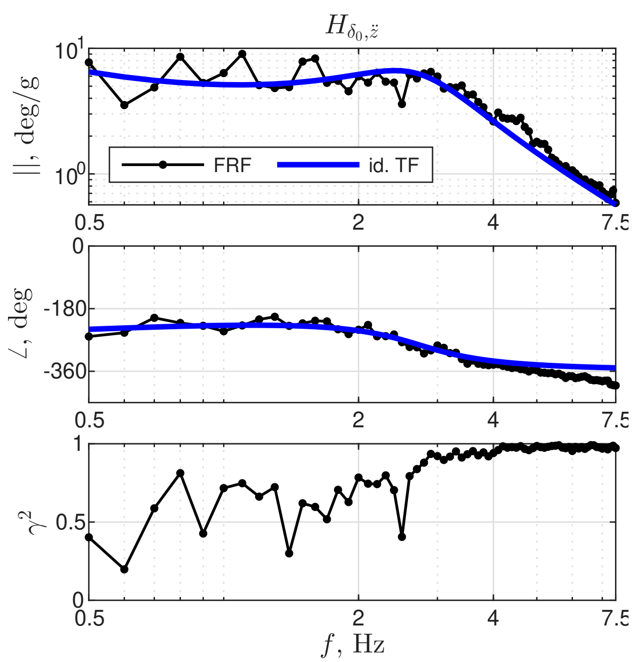

Figure 3. Experimental and identified BDFT transfer function for pilot PP-02. Experimental FRF: black line; identified BDFT transfer function: blue line.

Table 3. BDFT model parameters in Eq. (2) from identification on results of the three experiments with each pilot at 80 % collective (target position).

Parameter	NP-01	PP-02	Units
μ (run 1)	−10.95	−11.44	deg/g
μ (run 2)	−24.41	−2.18	deg/g
μ (run 3)	−21.70	−15.76	deg/g
T_z (run 1)	0.34	0.54	s
T_z (run 2)	0.17	2.59	s
T_z (run 3)	0.15	0.29	s
ξ (run 1)	0.29	0.47	–
ξ (run 2)	0.28	0.40	–
ξ (run 3)	0.34	0.32	–
ω_0 (run 1)	2.42	2.32	Hz
ω_0 (run 2)	2.65	2.44	Hz
ω_0 (run 3)	2.56	2.72	Hz

Preliminary Stability Assessment

The identified BDFTs were put in closed-loop with a simplified, linear time-invariant model of the helicopter vertical dynamics presented in previous publications (Refs. 11, 15). The simple, two-degrees-of-freedom model accounts for the airframe heave motion, z, and the main rotor collective flapping (coming) motion β_0. Both are intended as variations with respect to hover trim conditions. The forcing term is represented by the variation of the blade's collective pitch angle θ_0 with respect to trim conditions. The axial inflow dynamics have been neglected, as they do not significantly affect the helicopter's vertical response in the frequency range of interest. The equations of motion, in matrix form, are the following:

$$\mathbf{M}\Delta\ddot{\mathbf{x}} + \mathbf{C}\Delta\dot{\mathbf{x}} + \mathbf{K}\Delta\mathbf{x} = \mathbf{F}\Delta\theta_0 \tag{3}$$

where

$$\mathbf{M} = \begin{bmatrix} m_h & N_b S_b \\ N_b S_b & N_b I_b \end{bmatrix} \tag{4}$$

$$\mathbf{C} = \frac{1}{24R^2} N_b \gamma \Omega I_b \begin{bmatrix} 6 & 4R \\ 4R & 3R^2 \end{bmatrix} \tag{5}$$

$$\mathbf{K} = N_b \Omega^2 I_b \begin{bmatrix} 0 & 0 \\ 0 & \hat{\nu}_\beta^2 \end{bmatrix} \tag{6}$$

$$\mathbf{F} = \frac{1}{24R} N_b \Omega^2 \gamma I_b \begin{bmatrix} 4 \\ 3R \end{bmatrix} \tag{7}$$

and $\mathbf{x}^T = \left\{\Delta z \quad \Delta\beta_0\right\}$.
The corresponding state-space representation is derived, with the vertical acceleration, $\Delta\ddot{z}$, as output, and the collective blade pitch, θ_0, as the input. Table 4 lists the parameters utilized in the stability analysis, representative of a medium/light-weight, five-bladed main rotor configuration.

The flapping frequency is $\omega_\beta = 5.83\,\text{Hz}$. In the Laplace domain, the helicopter dynamics are given by:

$$\Delta\ddot{z} = H_{\ddot{z}\theta_0}(s)\Delta\theta_0 \tag{8}$$

Table 4. Helicopter model data. Lift-slope coefficient $a = 2\pi$ and air density $\rho = 1.255\,\text{kg}\,\text{m}^{-3}$ are used throughout. The blade static moment and moment of inertia are estimated considering uniform mass distribution $S_\beta = 1/2 M_b R$, $I_\beta = 1/3 M_b R^2$.

Parameter	Symbol	Value	Units
Mass	m_h	4000	kg
Number of Blades	N_b	5	–
Rotor Radius	R	6.0	m
Rotor Speed	Ω	330.0	rpm
Blade Mass	M_b	40.0	kg
Blade Chord	c	0.4	m
Lock Number	γ	8.3	–
Flap Static Moment	S_β	120.0	kg m
Flap Inertia Moment	I_β	480.0	$\text{kg}\,\text{m}^2$
Flap Frequency (adim.)	ν_β	1.040	–
Pitch-Flap Coupling	δ_3	15.0	°
Landing Gear Stiffness	K_t	6.47×10^5	$\text{N}\,\text{m}^{-1}$
Landing Gear Damping	C_t	6.18×10^3	$\text{N}\,\text{s}\,\text{m}^{-1}$

Neglecting the control chain dynamics completely, the collective blade pitch variation $\Delta\theta_0$ can be related to the collective inceptor rotation δ_0 by a simple gain G, i.e., the gear ratio representing the static kinematic relationship between the two angles:

$$\Delta\ddot{z} = H_{\ddot{z}\theta_0}(s)G\Delta\delta_0 \tag{9}$$

The total control deflection δ_0 can be split into a *control-motivated* contribution $\delta_{0,\text{cm}}$ and a *control-unrelated* $\delta_{0,\text{cu}}$ contribution (Ref. 16). The former is the contribution the pilot utilizes for guidance and mission-related tasks, while the latter is mainly due to the biomechanical response of the pilot's body, and can thus be seen as related, through the BDFT, to acceleration in the heave direction:

$$\delta_0(s) = \delta_{0,\text{cm}}(s) + \delta_{0,\text{cu}}(s) = \delta_{0,\text{cm}}(s) + H_{\text{BDFT}}\ddot{z} \tag{10}$$

Substituting in Eq. (8):

$$(1 - H_{\ddot{z},\theta_0}(s)GH_{\text{BDFT}})\ddot{z}(s) = H_{\ddot{z}\theta_0}(s)G\delta_{0,\text{cm}}(s) \tag{11}$$

Therefore, the closed-loop transfer function $H_{\text{CL}}(s)$ and the open-loop transfer function $H_{\text{OL}}(s)$ are:

$$H_{\text{CL}}(s) = \frac{\ddot{z}(s)}{\delta_{0,\text{cm}}(s)} = \frac{H_{\ddot{z},\theta_0}(s)G}{1 - H_{\ddot{z},\theta_0}(s)GH_{\text{BDFT}}} \tag{12}$$

$$H_{\text{OL}}(s) = -H_{\ddot{z},\theta_0}(s)GH_{\text{BDFT}} \tag{13}$$

The Gain Margin (GM) and Phase Margin (PM) of the loop transfer function H_{OL} were adopted as indicators of the PVS stability. The former is defined as the inverse of the magnitude of the LTF at the *crossover frequency* ω_{180}, i.e., the frequency at which the Nyquist plot crosses the negative real axis between -1 and 0. The Phase Margin can instead be defined as the amount of negative phase that can be added to the loop transfer function at the crossover frequency before the phase at ω_{180} becomes $-180°$, which corresponds to the closed-loop stability limit (Ref. 17).

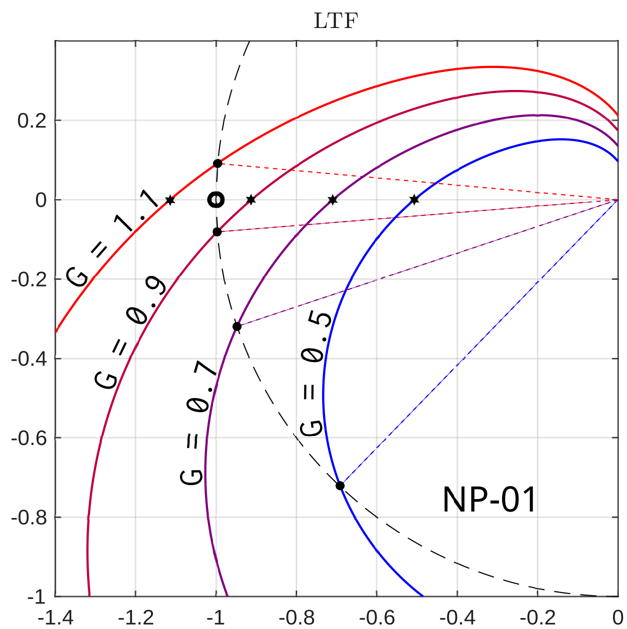

Figure 4. Nyquist plot of the loop transfer function for the pilot-vehicle with NP-01's BDFT, with varying gear ratio G between the collective lever rotation δ_0 and the blade's collective pitch θ_0.

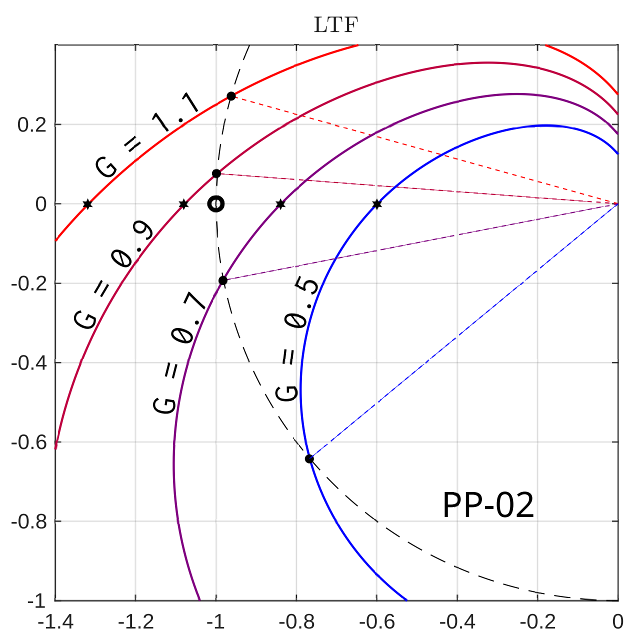

Figure 5. Nyquist plot of the loop transfer function for the pilot-vehicle with PP-02's BDFT. From blue to red, the gear ratio G increases from the nominal value, 0.5, to 1.1.

Table 5. Results of the closed-loop stability analysis of the PVS, for the pilots participating in the trials.

Pilot	G	GM_1	GM_2	GM_3	PM_1	PM_2	PM_3
NP-01	0.5	5.9	4.1	5.8	46.4	41.7	123.0
NP-01	0.7	3.0	1.2	2.9	18.6	8.1	21.4
NP-01	0.9	0.8	-1.0	0.7	4.6	-6.2	4.6
NP-01	1.1	-0.9	-2.8	-1.0	-5.3	-15.8	-6.4
PP-02	0.5	6.0	5.5	4.5	51.5	45.1	39.9
PP-02	0.7	3.0	2.6	1.5	23.1	19.4	11.0
PP-02	0.9	0.9	0.4	-0.7	6.4	3.1	-4.4
PP-02	1.1	-0.9	-1.3	-2.4	-6.6	-9.7	-15.8

The results of the stability analyses are summarized in Table 5 and the Nyquist diagrams in Figures 4 and 5.

Small but significant differences are visible in the stability margins progression from more stable conditions, at lower gear ratio factors, to less stable and unstable conditions at higher values of G. On average, though, the two pilots exhibit similar behavior, with the predicted critical value of G, separating stable and unstable conditions, found near $G = 1.0$ for both pilots.

This result seems to contradict, at least in part, past experiences, considering that the two pilots taking part in the experimental trials exhibit significantly different body types (Cf. Table 2). Past results (Refs. 6, 18, 19) suggested the presence of correlation between the pilots' anthropometrics and their contribution to the stability of the PVS. While noting that past studies either identified the pilot BDFT from a single experimental trial or via numerical simulation, preventing the assessment of the statistical scattering of pilot response, this is a topic surely worth further investigation.

CLOSED-LOOP EXPERIMENTS

Having conducted the preliminary stability analysis, an experimental campaign has been conducted on the RPC testbed, featuring simulated flight experiments. Two virtual scenarios have been developed:

1. an Instrument Meteorological Conditions (IMC) flight, requiring the pilots to maintain leveled flight conditions only relying on flight instruments readings, while subjected to external disturbances;
2. an ADS-33 vertical repositioning maneuver (VRM), requiring the pilots to acquire and maintain a target altitude, aided by specific visual elements.

Real-Time Flight Simulation Setup

The pilot-in-the-loop simulation was performed using the MARSH framework (Ref. 20), a system for connecting loosely coupled software modules into a research flight simulator. The system is based on the MAVLink protocol (Ref. 21), developed for unmanned vehicles, and is published as open-source software.

Flight Dynamics Model

The same model of the helicopter's heave and collective flap dynamics presented in Section Preliminary Stability Assessment was implemented in MATLAB Simulink, representing the Flight Dynamics Module (FDM). The only input to the model is the collective blade pitch angle θ_0, controlled linearly through the collective lever position. In order to ensure that the pilot is in the correct body pose, the collective input is measured relative to a desired trim position. Based on the typical hover operation of helicopters in this class, that value was set to 70 % of total lever travel from the bottom end stop, and displayed to the pilot alongside current collective position. The pilot has been asked to manually track the trim collective input at the beginning of each simulated flight. No ground effect has been considered in the FDM affecting rotor lift, but a simple ground contact model was implemented. This was done by including the terms for landing gear stiffness K_t and viscous damping C_t from the original formulation for a landed helicopter, but only when the height z was lower than 0. This can be interpreted as settling into the landing gear and has the desired effect of only ever providing upward force.

Virtual Visual Cueing

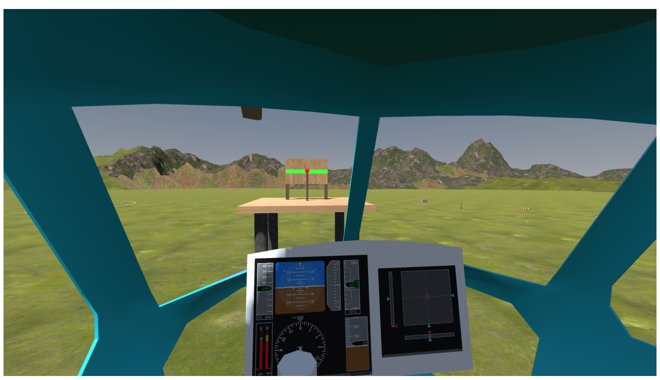

Figure 6. The VR visualisation depicting the pilot's view in front of the vertical position reference.

The visualization module was developed by the authors using the open-source video game engine Godot (Ref. 22). The complete source code and assets are available under the MIT license (Ref. 23). The pilot view can be displayed on a regular computer screen and/or using an OpenXR-compatible headset. Specifically, the Varjo XR-3 was used for the experiments. To correctly position the viewpoint inside the cockpit, the motion platform movement is also tracked by the VR hardware (using Vive Tracker 3.0), and its relative transform is subtracted from the headset position in a stationary reference frame. The environment contains all the ground features suggested in ADS-33 (Ref. 24). Considering that only the heave movement can be performed, Section *3.11.6 Vertical Maneuver* is most relevant. As suggested by the standard, the vertical position has a visual "hover board" reference at each target altitude (15 ft and 40 ft), which consists of a red sphere in front of a board with a green line, as seen in figure 6. The parallax effect causes the center of the sphere to leave the board at an error of ± 1.5 ft, which was adjusted from the standard's desired ± 3.3 ft in the course of experiments, to compensate for the absence of additional tasks.

Performed Tests

Two scenarios were developed for the initial phase of closed-loop testing:

1. an Instrument Meteorological Conditions flight;
2. an ADS-33 vertical repositioning maneuver.

During stationary flight phases, band-limited (0.5 Hz–7.5 Hz[1]) white noise acceleration signals are injected into the cockpit via the motion platform to enable the estimation of the frequency response function connecting the rotation of the control inceptors to the input acceleration, and thus the subsequent identification for the BDFT.

IMC Tests

At the time of writing, only preliminary results are available for the first scenario, which was developed mainly to allow closed-loop identification of the pilot BDFT, to validate the experimental procedures usually followed in open-loop tests (Refs. 7, 11). Specifically, the research questions these tests are aimed at answering are:

i is the biomechanical response of the pilots' bodies altered significantly by the change of task, from piloting to simply tracking a desired command position?

ii if the response to i is yes, how, and how much?

iii if the response to i is yes, can the results of open-loop identification still be useful (e.g., because they lead to conservative choices) in the design of RPC-free rotorcraft?

The path envisioned to answer these questions is to perform closed-loop identification of the pilot BDFT during simulated flight experiments. The trials should contain significant portions of steady-state conditions to facilitate the identification process, and the test platform must be able to provide motion cueing and a controllable external excitation source. The RPC platform is capable of providing the required inputs.

At the time of writing, only the results of preliminary tests, performed with only one pilot, PP-02, and without motion cueing, are available and will be presented here.

The tests were conducted closing the piloting loop with only visual cueing provided by a virtual Primary Flight Display,

[1]Signal generator implementation: https://github.com/marsh-sim/sim-nodes/blob/main/extra_waveform.py

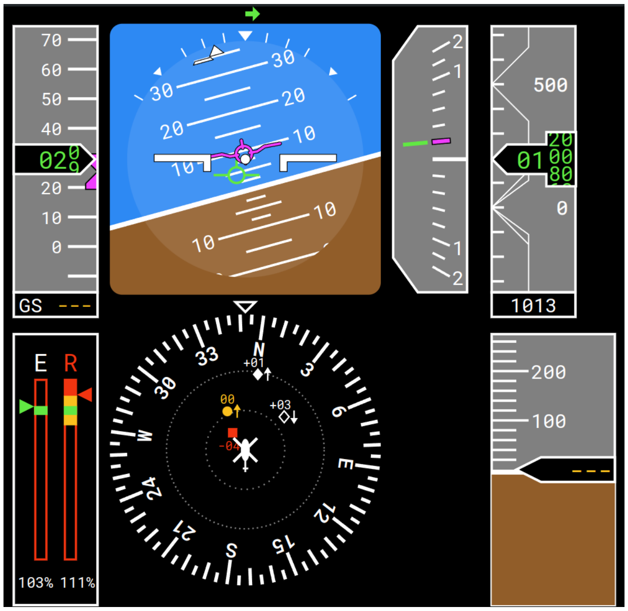

Figure 7. Virtual Primary Flight Display (PFD) available to pilots during IMC tests.

shown in Fig. 7. Each trial lasted 120 s. The pilot was instructed to maintain the initial flight conditions, i.e., leveled flight at 1000 ft altitude and 60 kn IAS. No motion cueing was introduced by the motion platform, which only provided a white noise input in the band 0.5–7.5 Hz[2]), with $1.0\,\mathrm{m\,s^{-2}}$ RMS amplitude, identical to the one utilized for open-loop BDFT identification. In the initial 60 s of simulation, no external disturbances acted on the aircraft. In the last 60 s of the trial, a moderate turbulence, following Dryden's model, was introduced, providing an increase in the task difficulty. The intensity of the gust was set to produce maximum wind speeds not exceeding 15 kn. Figure 8 shows the identified BDFTs in two subsequent runs, in the green and purple lines, compared to transfer functions identified with standard procedures, i.e., with collective position tracking tasks and white noise vertical acceleration input, in the blue and orange lines. During open-loop identification, the pilots were instructed to utilize either a *standard* gripping on the collective lever, holding it as tight as comfortable, or asking them to hold the inceptor as tight as possible. In principle, this should provide the identification of the full range of possible pilots' body responses. However, it can be seen that the transfer functions identified during the simulator trials differ from the ones identified during the open-loop tests.

Specifically, it can be seen that the transfer functions identified during the IMC runs — both the ones identified in the first 60 s, shown in black with crosses, and the ones identified in the last 60 s, shown in black with circular markers — are characterized by a marked reduction in the damping of the main biomechanical pole, with respect to the open-loop identifications. The frequency of the pole lies, instead, between those

[2] Signal generator implementation: https://github.com/marsh-sim/sim-nodes/blob/main/extra_waveform.py

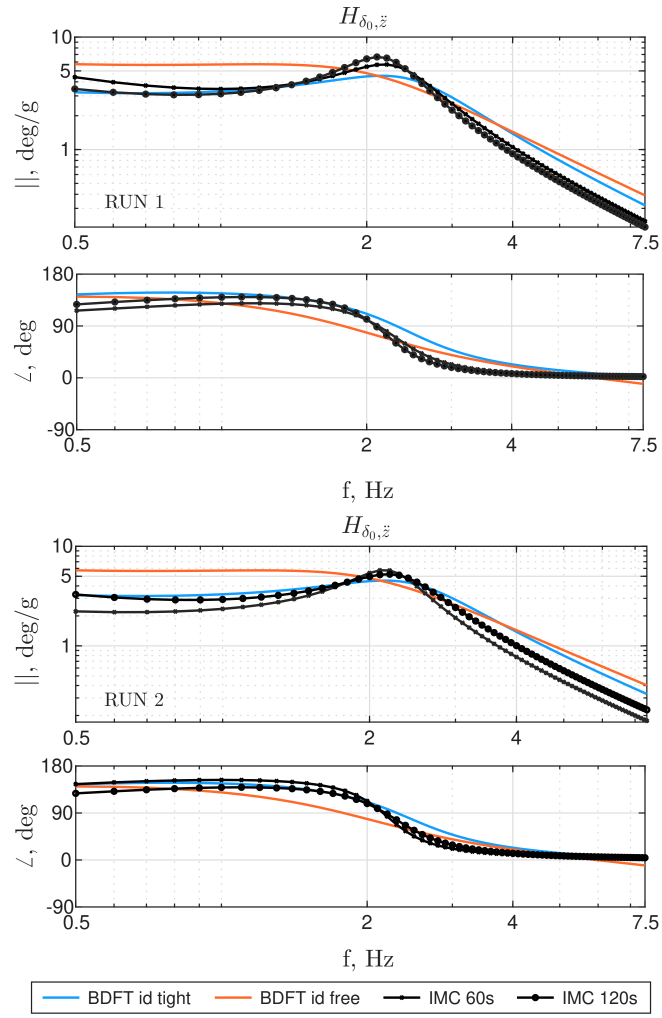

Figure 8. BDFTs identified in IMC scenario (black lines), with pilot-in-the-loop and without motion cueing, compared to BDFTs identified in standard open-loop tests, with *tight* (blue lines) and *free* (red lines) gripping. Results from two simulator runs: RUN 1 (top), RUN 2 (bottom).

of the *free* and *tight* gripping open-loop identification.

From these very preliminary tests, it would seem that the response to research question i is "yes," as a further confirmation of previous results (Refs. 3, 5). The initial answers to questions ii and iii would seem to be "significantly" and "no," but they can only be answered after a more extensive analysis. They have been purposely given in a very qualitative flavor to underline that no hard conclusions can be drawn at this time. In fact, a different trend regarding question iii has been found in the tests described in the next Section, VERTICAL REPOSITIONING MANEUVER.

More tests, both with the same pilot and with different pilots, are needed to confirm the observed behavior and assess the impact of the discrepancies on the stability of the PVS. At the present time, this finding represents, more than anything else, an interesting hint for a line of research to be pursued further.

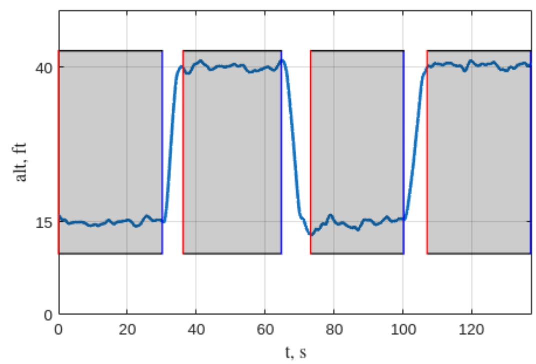

Figure 9. Time history of the helicopter altitude during one of the simulator trials. The shaded sections correspond to “HOLD” MTEs, while the “TRANSITION” MTEs are in between them.

VERTICAL REPOSITIONING MANEUVER

In the following sections, the focus is placed on the second developed scenario, representing an ADS-33 Vertical Repositioning Maneuver. The virtual environment for this task has been presented in Section Virtual Visual Cueing: the pilots are immersed in a virtual environment containing two hover boards, one placed at 15 ft and the other at 40 ft, and were asked to perform the following Mission Task Elements:

1. maintain the 15 ft altitude, for 30 s;
2. transition to the 40 ft target, in approximately 5 s;
3. maintain the 40 ft altitude, for 30 s;
4. transition to the 15 ft target, in approximately 5 s;
5. maintain the 15 ft altitude, for 30 s;
6. transition to the 40 ft target, in approximately 5 s;
7. maintain the 40 ft altitude, for 30 s.

In total, 4 stationary sections (“HOLD” MTEs) are interleaved with 3 repositioning (”TRANSITION” MTEs) maneuvers. The latter were initiated by communicating to the pilot via intercom: a countdown of 3 seconds preceded the signal to initiate the maneuver, followed by a countdown of 5 seconds to indicate the target time for the maneuver completion. Figure 9 shows an example time history of the altitude during one of the trials.

During the simulated flights, motion cueing was provided by the testbed platform. Each test point was repeated twice; then the value of the gear ratio G was updated. The same values utilized in open-loop stability analysis were also set for the simulated flight tests: 0.5, 0.7, 0.9, 1.1. For pilot PP-02, also $G = 1.3$ was tested, as discussed in the next Section.

The research questions that the experimental trials were designed to address are the following:

I are the stability boundaries predicted by the offline simulations, like the one outlined in Section Preliminary Stability Assessment, confirmed in (simulated) flight?

II if the answer to I is “no,” is the offline stability assessment conservative?

Note that several other questions could be added to these core ones. Some examples will be given in Section CONCLUSIONS. Question I is tightly connected to question 1: if the dynamic response of the pilot body during simulated flight test is consistent with the one it exhibits during open-loop testing, the identifications performed during the open-loop testing are representative and can be safely employed in the stability analysis for design purposes. Another possible scenario is that they represent a conservative measure of the pilot’s participation in the closed-loop dynamics, meaning that a stability analysis employing them is bound to give consistently worse stability margins with respect to the flight conditions. It is a possibility that has surfaced in past studies (Ref. 2), but has not been further investigated in recent studies.

Results

During the simulated trials, no severe instabilities occurred in the form of exponentially growing oscillations or limit cycles with large amplitudes. This is in contrast with the predictions of the offline stability analysis, which indicated for both pilots negative, in some cases significantly negative, stability margins for $G > 1.0$. Pilot NP-01 experienced some small amplitude sustained vibrations at gear ratio $G = 0.9$, and some small to moderate amplitude oscillations with gear ratio $G = 1.1$. Pilot PP-02 experienced some oscillations at $G = 1.1$ and $G = 1.3$, in both cases of amplitudes smaller than those of NP-01.

The collective rotation signals were analyzed in the time and frequency domain, applying a Continuous Wavelet Transform (CWT) based on the Bump wavelet. The resulting scalograms are shown in Figures 10, 11, 12, 13. Vertical white lines indicate the beginning (dashed) and end (dotted) of “HOLD” MTEs.

The corresponding scalograms for pilot PP-02 are shown in Figures 14, 15, 16, 17 and 18. It can be clearly seen that the energy content of the collective rotation is increasing in the frequency band associated with the dominant BDFT pole, i.e., 2 Hz–3 Hz. This suggests that the stability of the PVS is decreasing, and the appearance of light to moderate — the latter especially in the case of NP-01 — oscillations was noted during the experimental trials. Pilot NP-01 also noted that the oscillations increased when he tried to relax the left arm, suggesting perhaps that the muscular tension building in the limb muscles, due to the more representative piloting task and the necessity to increase the control inceptor movement precision, has a positive effect on the PVS stability.

More data analysis, and more tests, are needed to confirm the results and to form a complete picture able to fully justify the

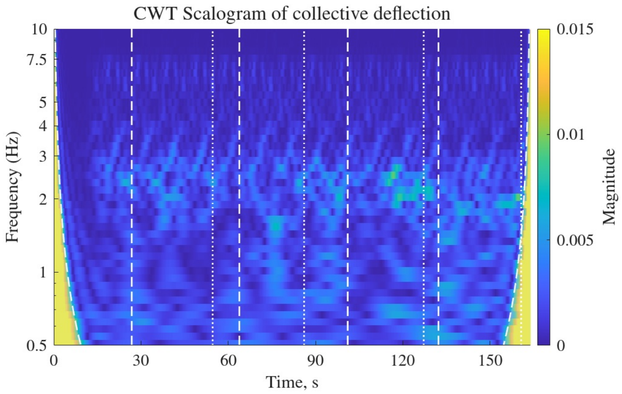

Figure 10. Scalogram of the collective inceptor rotation during the simulated vertical repositioning maneuvers of pilot NP-01. The gear ratio for the trial was set at $G = 0.5$.

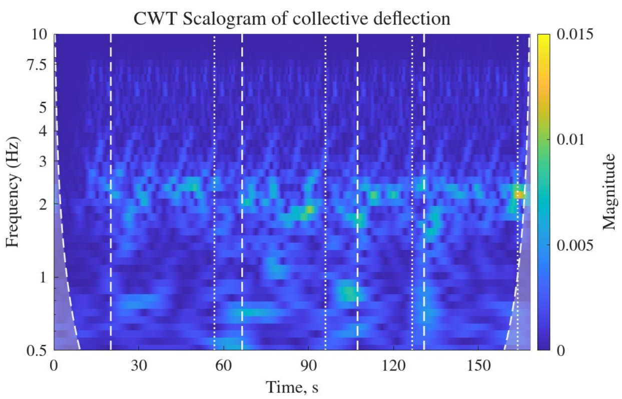

Figure 11. Scalogram of the collective inceptor rotation during the simulated vertical repositioning maneuvers of pilot NP-01. The gear ratio for the trial was set at $G = 0.7$.

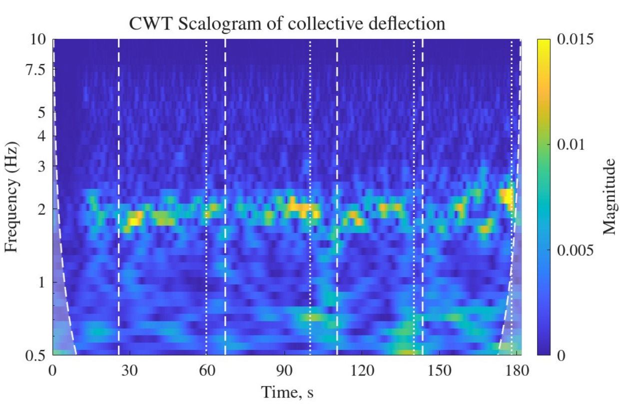

Figure 12. Scalogram of the collective inceptor rotation during the simulated vertical repositioning maneuvers of pilot NP-01. The gear ratio for the trial was set at $G = 0.9$.

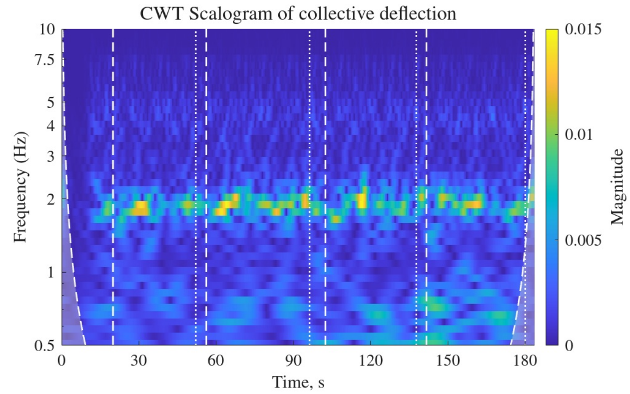

Figure 13. Scalogram of the collective inceptor rotation during the simulated vertical repositioning maneuvers of pilot NP-01. The gear ratio for the trial was set at $G = 1.1$.

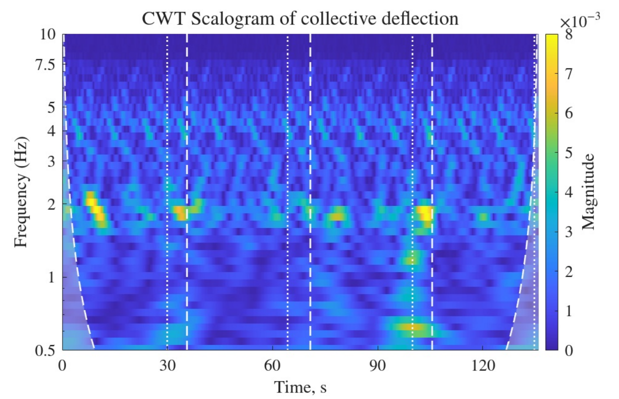

Figure 14. Scalogram of the collective inceptor rotation during the simulated vertical repositioning maneuvers of pilot PP-02. The gear ratio for the trial was set at $G = 0.5$.

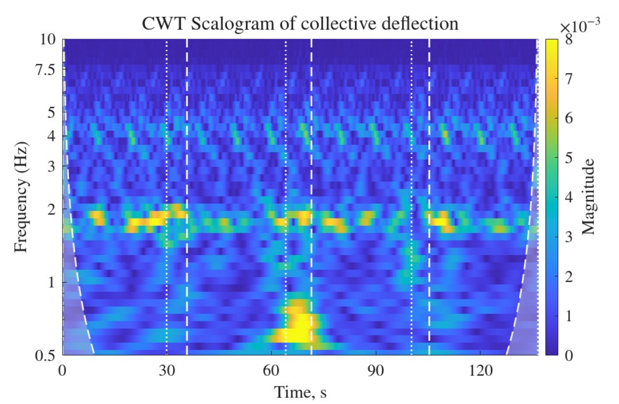

Figure 15. Scalogram of the collective inceptor rotation during the simulated vertical repositioning maneuvers of pilot PP-02. The gear ratio for the trial was set at $G = 0.7$.

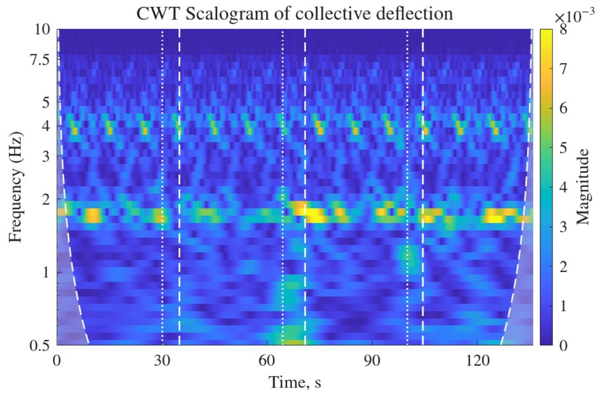

Figure 16. Scalogram of the collective inceptor rotation during the simulated vertical repositioning maneuvers. The gear ratio for the trial was set at $G = 0.9$.

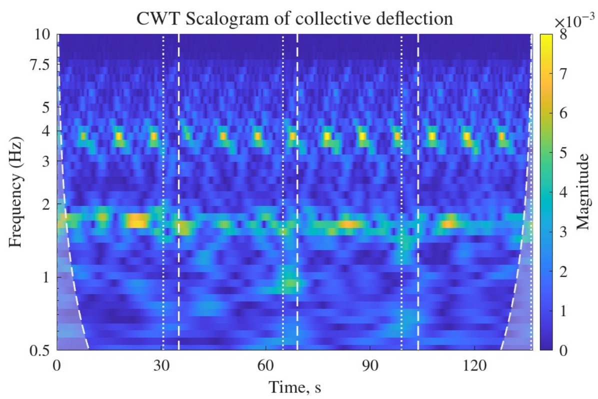

Figure 17. Scalogram of the collective inceptor rotation during the simulated vertical repositioning maneuvers. The gear ratio for the trial was set at $G = 1.1$.

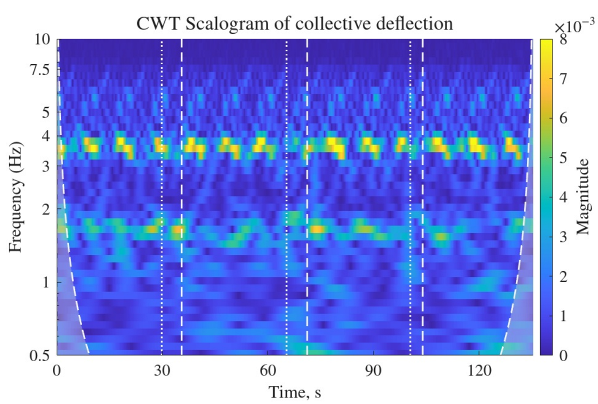

Figure 18. Scalogram of the collective inceptor rotation during the simulated vertical repositioning maneuvers. The gear ratio for the trial was set at $G = 1.3$.

observed trends, but from the preliminary analysis here presented the answer to question I would seem to be "no" or at least "not fully," but in this case the answer to the subsequent question II would seem to be "yes," as already found also in previous experiences (Ref. 10).

CONCLUSIONS

The presented experimental setup has allowed the initiation of a systematic study on the effect on Rotorcraft-Pilot Couplings of the piloting tasks and on the quantification of the robustness of the *traditional* approach of relying on open-loop BDFT identifications to introduce the pilot biomechanical response in the PVS closed-loop stability analysis. The RPC testbed is now actively being exploited for simulated flight tests in scenarios that can potentially trigger RPC events, and will be utilized for the same purpose with increasing effort moving forward.

The initial results of the first two experiments, featuring Instrument Meteorological Conditions flight and an ADS33 Vertical Repositioning Maneuver scenario, indicated that the task has a significant influence on the pilot's BDFT. Furthermore, no conclusive evidence was found concerning the *direction* of the change, from tracking tasks employed in open-loop testing to full piloting tasks employed in closed-loop simulator trials. From the more comprehensive set of tests, i.e., the ADS33 VRM trials, some confirmation that relying on open-loop testing represents a conservative path towards RPC-free design has been found, but the same cannot be said for the IMC test trials. More investigation is thus necessary, starting from completing and extending the comparison between the offline stability analysis on the PVS model and the experimental findings on the simulator trials.

Future Developments

Aside from the generic considerations made in the previous Section on the importance of extending the experimental campaign, both in terms of trials per pilot and in the number of tested (professional and non-professionally trained) pilots, some improvements to the current setup and methodologies are envisioned:

1. perform BDFT identifications tests based on the developed ADS33 vertical repositioning task, without including motion cueing: this will allow to isolate the effect of the task on the BDFT;
2. improve the experimental setup to include also means to collect data on the pilot body pose, allowing to confirm that it is not varied significantly from open-loop tests to closed-loop tests;
3. better understand the role of the first axial mode of the spine, responsible for the relative amplification of the BDFT at 4–6 Hz, more evident for NP-01 (Cf. Figure 3), on the stability of the PVS;

4. perform simulator trials and open-loop identification tests with Electromyography (EMG) sensors applied to the pilot's left arm muscles, to compare their activity in the two contexts and allow for a quantitative evaluation of the differences in the biomechanical response.

Addressing these issues is expected to provide a more comprehensive understanding of the physical phenomena related to RPC and eventually lead to the development of guidelines for the robust design of rotorcraft human-machine interfaces and for pilot training for avoidance and management of RPC events.

Author contact: Andrea Zanoni andrea.zanoni@polimi.it

REFERENCES

1. Marilena D. Pavel, Michael Jump, Binh Dang-Vu, Pierangelo Masarati, Massimo Gennaretti, Achim Ionita, Larisa Zaichik, Hafid Smaili, Giuseppe Quaranta, Deniz Yilmaz, Michael Jones, Jacopo Serafini, and Jacek Malecki. Adverse rotorcraft pilot couplings—Past, present and future challenges. *Progress in Aerospace Sciences*, 62:1–51, October 2013.

2. Marilena D. Pavel, Pierangelo Masarati, Massimo Gennaretti, Michael Jump, Larisa Zaichik, Binh Dang-Vu, Linghai Lu, Deniz Yilmaz, Giuseppe Quaranta, Achim Ionita, and Jacopo Serafini. Practices to identify and preclude adverse Aircraft-and-Rotorcraft-Pilot Couplings – A design perspective. *Progress in Aerospace Sciences*, 76:55–89, July 2015.

3. Joost Venrooij, David A. Abbink, Mark Mulder, Marinus M. van Paassen, and Max Mulder. Biodynamic feedthrough is task dependent. In *2010 IEEE International Conference on Systems, Man and Cybernetics*, pages 2571–2578, Istanbul, Turkey, October 2010. IEEE.

4. Joost Venrooij, David A. Abbink, Mark Mulder, Marinus M. van Paassen, and Max Mulder. A Method to Measure the Relationship Between Biodynamic Feedthrough and Neuromuscular Admittance. *IEEE Transactions on Systems, Man, and Cybernetics, Part B (Cybernetics)*, 41(4):1158–1169, August 2011.

5. Andrea Zanoni, Matteo Zago, Rita Paolini, Giuseppe Quaranta, Manuela Galli, and Pierangelo Masarati. On Task Dependence of Helicopter Pilot Biodynamic Feedthrough and Neuromuscular Admittance: An Experimental and Numerical Study. *IEEE Transactions on Human-Machine Systems*, 51(5):421–431, October 2021.

6. Vincenzo Muscarello, Giuseppe Quaranta, Pierangelo Masarati, Linghai Lu, Michael Jones, and Michael Jump. Prediction and Simulator Verification of Roll/Lateral Adverse Aeroservoelastic Rotorcraft–Pilot Couplings. *Journal of Guidance, Control, and Dynamics*, 39(1):42–60, January 2016.

7. A. Zanoni, D. Marchesoli, C. Talamo, P. Masarati, F. Colombo, S. Kemp, and E. Fosco. Experimental test-bed for the identification of biodynamic feedthrough of helicopter-pilot systems. In *48rd European Rotorcraft Forum, ERF 2022*, Winterthur, Switzerland, 2022-09-06/2022-09-08.

8. Joost Venrooij. *Measuring, Modeling and Mitigating Biodynamic Feedthrough.* PhD thesis, Technische Universiteit Delft, Delft, The Netherlands, 2014.

9. P. Welch. The use of fast fourier transform for the estimation of power spectra: A method based on time averaging over short, modified periodograms. *IEEE Transactions on Audio and Electroacoustics*, 15(2):70–73, 1967.

10. Pierangelo Masarati, Giuseppe Quaranta, Linghai Lu, and Michael Jump. A closed loop experiment of collective bounce aeroelastic Rotorcraft–Pilot Coupling. *Journal of Sound and Vibration*, 333(1):307–325, January 2014.

11. Andrea Zanoni, Gianni Cassoni, Carmen Talamo, Davide Marchesoli, Michele Zilletti, Francesca Colombo, and Pierangelo Masarati. An Uncertainty Propagation Approach to Collective Bounce Rotorcraft-Pilot Couplings Analysis. In *80th Vertical Flight Society Annual Forum and Technology Display, FORUM 2024*, Montréal, Quebec, Canada, May 2024. Vertical Flight Society.

12. Tommaso Aresi, Andrea Zanoni, Gianni Cassoni, and Pierangelo Masarati. Simplified models of pilot biomechanics for rotorcraft vertical bounce analysis. In *34th Congress of the International Council of the Aeronautical Sciences, ICAS 2024*, Florence, Italy, September 2024.

13. C Talamo, A Zanoni, T Aresi, P Masarati, E Fosco, and F Colombo. Decoupling pilot biomechanics from control device dynamics in biodynamic feedthrough: A multibody dynamics approach. In *50th European Rotorcraft Forum*, Marseille, France, 10–12 September, 2024.

14. Satoshi Kitazaki and Michael J Griffin. Resonance behaviour of the seated human body and effects of posture. *Journal of Biomechanics*, 31(2):143–149, May 1997.

15. Vincenzo Muscarello, Giuseppe Quaranta, and Pierangelo Masarati. The role of rotor coning in helicopter proneness to collective bounce. *Aerospace Science and Technology*, 36:103–113, 2014.

16. Davide Marchesoli, Andrea Zanoni, and Pierangelo Masarati. A meta-model for comprehensive pilot modeling. In *80th Vertical Flight Society Forum*, Montreal, Canada, May 7–9 2024. https://doi.org/10.4050/F-0080-2024-1272.

17. Sigurd Skogestad and Ian Postlethwaite. *Multivariable Feedback Control: Analysis and Design*, chapter 2. Wiley, Chichester, 2. ed., repr edition, 2010.

18. John R. Mayo. The involuntary participation of a human pilot in the helicopter collective control loop. In *15th European Rotorcraft Forum*, pages 81–001–012, Amsterdam, The Netherlands, September 1989.

19. Andrea Zanoni and Vincenzo Muscarello. Moving towards a-priori identification of undesirable pilot biometrics for collective bounce instability. In *43rd European Rotorcraft Forum, ERF 2017*, pages 773–787, 2017.

20. Marek S Lukasiewicz. Modular architecture for reconfigurable simulation of helicopters: Online documentation. https://marsh-sim.github.io, last accessed 2025-07-16.

21. Lorenz Meier and many al. Mavlink, micro air vehicle link protocol. https://mavlink.io/, last accessed 2025-07-15.

22. Juan Linietsky, Ariel Manzur, and Godot Engine contributors. Godot engine - free and open source 2d and 3d game engine. https://godotengine.org, 2007–2025.

23. Marek S Lukasiewicz and Margaux Touzard. Visualisation for MARSH. https://git.lukasiewicz.tech/DAER/visualisation-marsh, last accessed 2025-07-16.

24. ADS-33E-PRF, Aeronautical Design Standard, Performance Specification, Handling qualities Requirements for Military Rotorcraft, March 2000.